In adatom diffusion on $In_xGa_{1-x}As$/GaAs(001): effects of strain, reconstruction and composition

2009 J. Phys.: Condens. Matter 21 355007

(http://iopscience.iop.org/0953-8984/21/35/355007)

IOP PUBLISHING JOURNAL OF PHYSICS: CONDENSED MATTER

J. Phys.: Condens. Matter **21** (2009) 355007 (9pp) doi:10.1088/0953-8984/21/35/355007

In adatom diffusion on $In_xGa_{1-x}As$/GaAs(001): effects of strain, reconstruction and composition

M Rosini[1], P Kratzer[2] and R Magri[1]

[1] Dipartimento di Fisica, Università degli Studi di Modena e Reggio Emilia and S3 Research Center of CNR-INFM, via Campi 213/A, 41100 Modena, Italy
[2] Fachbereich Physik and Center for Nanointegration (CeNIDE), Universität Duisburg-Essen, Lotharstrasse 1, 47048 Duisburg, Germany

E-mail: marcello.rosini@unimore.it

Received 21 April 2009, in final form 30 June 2009
Published 7 August 2009
Online at stacks.iop.org/JPhysCM/21/355007

Abstract

By using density functional theory (DFT) calculations of the potential energy surface in conjunction with the analytical solution of the master equation for the time evolution of the adatom site distribution, we study the diffusion properties of an isolated In adatom on $In_xGa_{1-x}As$ wetting layers (WL) deposited on the GaAs(001). The WL reconstructions considered in this study are, listed in the order of increasing In coverage: c(4 × 4), (1 × 3), (2 × 3), α_2(2 × 4) and β_2(2 × 4). We analyze the dependence of the diffusion properties on WL reconstruction, composition and strain, and find that: (i) diffusion on the (2 × N) reconstructions is strongly anisotropic, owing to the presence of the low barrier potential in-dimer trench, favoring the diffusion along the [$\bar{1}$10] direction over that along the [110] direction; (ii) In diffusion at a WL coverage $\theta = 2/3$ monolayers (ML; with composition $x = 2/3$) is faster than on clean GaAs(001) c(4 × 4), and decreases at $\theta = 1.75$ ML ($x = 1$; e.g. InAs/GaAs(001)); (iii) diffusion and nucleation on the (2 × 4) WL is affected by the presence of adsorption sites for indium inside the As dimers; (iv) the approximation used for the exchange–correlation potential within DFT has an important effect on the description of the diffusion properties.

(Some figures in this article are in colour only in the electronic version)

1. Introduction

Adatom diffusion on semiconductor surfaces is a fundamental topic in nanostructure physics and technology: it is at the basis of the mechanisms of nucleation and growth of semiconductor nanostructures. Among semiconductor nanostructures, quantum dots and quantum wires have been widely studied, owing to their electronic and optical properties, that are of great interest both for basic science and for technological applications. Quantum dots exhibit atomic-like energy spectra, that can be tuned by controlling their growth process and, thus, can be optimized for specific purposes. On the other hand, free-standing nanowires can also be easily grown by MBE and, also in this case, the growth can be controlled to obtain ideal defect- and strain-free core–shell and axial heterostructures.

Nanostructure growth control can be achieved by growth protocols where the molecular flux and/or the growth temperature are varied in time. Here, we address the InGaAs/GaAs system. The growth process follows a Stranski–Krastanov growth mode [1], where the strain due to the InAs and GaAs lattice mismatch is relieved by forming first a wetting layer (WL), then 3D islands. The InGaAs WL on GaAs is compressively strained in the surface plane, and the strain is mainly relieved along the growth direction. When the WL thickness reaches a critical value (dependent on the WL composition), nucleation spontaneously occurs at the surface. At the onset of nucleation a significant mass transport takes

place. This is testified by the observation that the total volume of the formed 3D structures is much larger than the total volume of the deposited material [2]. Mobile indium atoms have been observed before the formation of the first nuclei [3]. The coordinated adsorbate motion during mass transport is thought to be originated by an ensemble of single surface diffusion events [4]. Thus, the study of the single adatom surface diffusion is a first fundamental step for understanding the nucleation mechanism which is an essential ingredient for achieving control of the growth process, and hence of the dot density and arrangement. Also, the growth regime of nanowires is governed by the ratio between In diffusion length on the surface and on the nanowire sidewalls [5].

In this work, we address In diffusion at the onset of the 2D $\rightarrow$ 3D transition. We focus our attention mainly to particularly In-rich WLs on GaAs(001), with a (2×4)(001) surface reconstruction, which was reported in the literature [4, 6–8] as the observed reconstruction of the WL at the onset of quantum dot formation. The transition takes place at $\theta \approx 1.7$ ML coverage, with $x = 0.8$ In surface composition [9, 10]. For a (001) In-rich surface the stable (2×4) reconstructions have been found to be α_2 and β_2 [11–13]. Both reconstructions consist of As dimers in the topmost, incomplete surface plane ('ad-dimers'), and As dimers formed from the As atoms of the complete As layer of the crystal ('in-dimers'). The β_2 contains an additional As ad-dimer, thus it is stabilized in a more As-rich atmosphere or/and at a lower growth temperature, where As evaporation from the surface is reduced. We compare the properties of In surface diffusion on the α_2 and β_2 reconstructions with those relative to reconstructions observed at lower In coverage regimes. Since the WL is subjected to compressive strain, we intend here to point out the effect of strain on In diffusion, by comparing our results with those for strain-free pure InAs surfaces reported previously in the literature [14].

It has been found [8] that as the In coverage increases, the (001) surface reconstruction changes from $c(4 \times 4)$ for pure GaAs, to (2×3) at a In $\theta \approx 0.7$ coverage, to finally a (2×4) reconstruction at a much higher In coverage. In the past, few theoretical investigations have been carried out for adsorption and diffusion on InGaAs surfaces, based on *ab initio* DFT calculations using mainly the GGA–PBE formulation for the exchange–correlation potential. Ga diffusion on GaAs $\beta_2(2 \times 4)$ was studied in [15], while diffusion on $c(4 \times 4)$ was addressed in [16]. Indium diffusion on the pure GaAs $c(4 \times 4)$ surface was addressed in [13] and on the (1×3) and $(2 \times 3)In_{0.66}Ga_{0.33}As$ wetting layers in [17]. Ishii *et al* [14] have calculated the adsorption sites and the effective barriers for In on the pure InAs $\beta_2(2 \times 4)$. Indium adsorption and diffusion on α_2 and $\beta_2(2 \times 4)$ InAs WLs on GaAs have been studied by us using a DFT–LDA formalism in [18, 19]. From these works it can be evidenced that the diffusion anisotropy is strongly related to the particular surface reconstruction and its symmetry: on the $(2 \times N)$ surfaces the diffusion is strongly anisotropic, while it is more isotropic on the $c(4 \times 4)$ reconstructed surface.

In this paper we compare diffusion on the different reconstructed InGaAs WLs pointing out the relation existing between In diffusion properties and the WL composition, reconstruction and strain situation.

The paper is organized as follows: in section 2 we describe the method used for the calculation of the diffusion properties of In on the WLs; in section 3 the results obtained are presented and discussed, in particular how WL composition and strain affect diffusion; in section 4 we compare with the previous results and experiment and finally, in section 5, we summarize and conclude.

2. Method

In order to compare In diffusion on the different reconstructed surfaces, we performed first-principles calculations for the α_2 and β_2 reconstructions, within the density functional theory in the generalized gradient approximation (DFT–GGA) using the PBE exchange and correlation functional [20]. We have used norm-conserving pseudopotentials treating the outermost s- and p-shells of Ga, In and As as valence electrons, and the electronic wavefunctions were expanded in plane-waves, with a 15 Ryd kinetic energy cutoff. The energy cutoff has been tested in order to reach convergence for the lattice bulk properties of GaAs and InAs. The core-corrected atomic pseudopotentials have been tested on bulk Ga, In and As, where the determined equilibrium configurations and elastic moduli compare well with the experimental data.

The equilibrium lattice parameters obtained for the GaAs and InAs bulk phases are $a_0 = 5.779$ Å and $a_0 = 6.314$ Å, which are slightly higher than the experimental ones 5.653 and 6.058 Å, respectively. Thus, our calculated lattice mismatch is 9.3%, higher than the experimental value of 7.2%. This is going to overestimate the effects due to the WL strain.

Starting from the GaAs structure, we have set up the (001) oriented supercell containing 4 layers of GaAs, covered with 1.75 layers of InAs arranged according to the $\alpha_2(2 \times 4)$ and $\beta_2(2 \times 4)$ surface reconstructions. The lower layer of Ga atoms is kept fixed during the cell relaxation, in order to mimic the constraint due to the underlying semi-infinite bulk, and it is passivated with pseudo-hydrogen atoms of 1.25 electron charge. The slab is repeated along the (001) direction with a periodicity $5a_0$ and a separation of about 10 Å of vacuum. Brillouin-zone (BZ) integration was carried out using a set of special k-points equivalent to 16 points in the 1×1 surface BZ. A smearing of 0.01 Ryd has been used in order to deal with the possible metallization of the surface electronic structure.

The relaxed geometries for $\alpha_2(2 \times 4)$ and $\beta_2(2 \times 4)$ are shown in figure 1.

The potential energy surface (PES) of an In adatom is calculated by relaxing the adatom z coordinate together with all the surface degrees of freedom while the in-plane x, y coordinates are kept fixed. We have set up a grid of 64 points, corresponding to a mesh width of 1.4 Å, along the (110) and $(\bar{1}10)$ directions respectively, and for each point we have found the minimum energy configuration for the adsorbate plus surface. Then, we have interpolated the grid data with a bi-cubic spline algorithm in order to find the positions of the minima and the saddle points. The exact values of the minima have then been determined by further relaxing all the

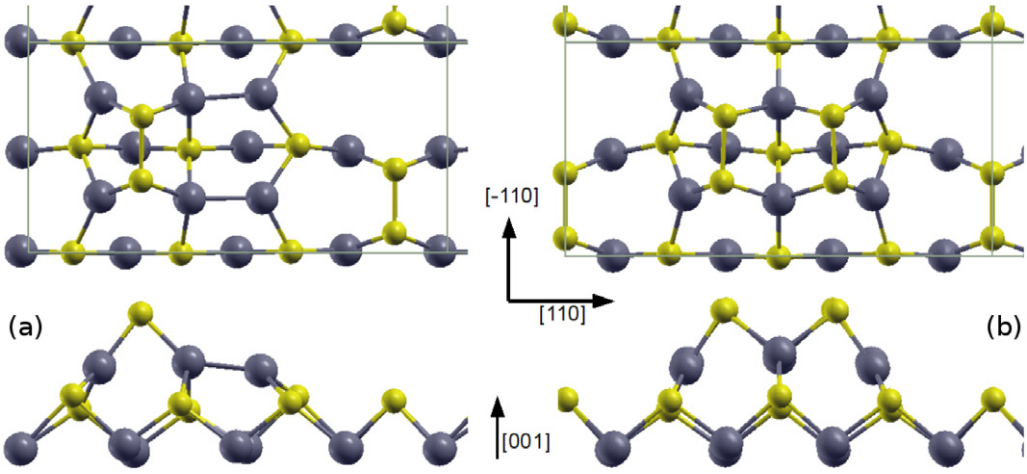

Figure 1. Representation of the $\alpha_2(2 \times 4)$ (a) and $\beta_2(2 \times 4)$ (b) surface reconstructions. The shown geometries are those optimized within the DFT–GGA approach. Note that the In–In bond in the top layer in the α_2 reconstruction is not parallel to the surface, but tilted. Dark balls and light balls represent In and As ions, respectively.

three coordinates of the adatom together with the surface. To minimize the spurious interaction between the adatom and its periodic images, we have doubled the surface unit cell along the $(\bar{1}10)$ direction.

These settings are used to calculate the potential energy surface for In diffusion *on top of* the WL. In addition, potential minima have been described in the literature [13, 15, 18] where the In adatom breaks the As dimers and inserts itself into them. In order to find the minimum energy paths (MEPs) connecting these minima to the other minima of the PES, we have performed calculations of the saddle points using the nudged elastic band method (NEB) [21]. This method is able to find the MEP between two adsorption sites, by simulating a string of replicas of the system, where the different images are linked by springs. By minimizing the energy associated to the path, an accurate description of the MEP and of the saddle point is obtained.

The diffusion motion originates from the random walk of the adsorbate on the surface, and consists of a series of thermally activated jumps. The adsorbate, starting from an initial adsorption state (j), after a given time τ, escapes to another adsorption site (k) with a transition probability per unit time $\Gamma_{kj} \equiv \Gamma_{k \leftarrow j} \equiv 1/\tau_{kj}$. The diffusion tensor is a function of the whole set of Γ_{kj}: this set defines the transition rate matrix [22].

In order to find the diffusion tensor we follow the method proposed in [23, 24], and previously used in [17]. The diffusion tensor is given by:

$$\mathbf{D} = \mathbf{B}\mathbf{H}\mathbf{B}^{\mathrm{T}}, \tag{1}$$

where $\mathbf{B}$ is the transformation matrix from Cartesian coordinates to lattice indices, $\mathbf{H}$ is the Hessian:

$$\mathbf{H} = -\tfrac{1}{2}\nabla_{\mathbf{q}}\nabla_{\mathbf{q}}\gamma_1(\mathbf{q})|_{\mathbf{q}=0}, \tag{2}$$

and $\gamma_1(\mathbf{q})$ [25] is the only eigenvalue of the transition state matrix such that $\gamma_1(0) = 0$.

The transition probabilities per unit time Γ_{kj} are obtained using transition state theory [26, 27], as:

$$\Gamma_{kj} = \Gamma_0 \mathrm{e}^{-\frac{\Delta U_{k,j}}{k_{\mathrm{B}}T}}, \tag{3}$$

where $\Delta U_{k,j}$ is the difference between the $T = 0$ K energy of the adsorption site k and that of the transition state at the saddle point along the $j \rightarrow k$ path, that is commonly referred to as diffusion barrier. Γ_0 is the so called attempt-to-escape frequency of the adatom and it is related to the vibrational properties of the system and to the temperature. In this work we assume $\Gamma_0 = 10^{13}$ s^{-1}, for each j, k, a value commonly used for these systems [11].

Another useful quantity for understanding diffusion is the mean permanence time in the binding site j, calculated as:

$$\tau_j = \left[\sum_k \Gamma_{kj}\right]^{-1}. \tag{4}$$

In order to calculate the diffusion tensor, we identify all the possible transitions from site j to the other sites k on the surface and find the transition probabilities per unit time Γ_{kj} (3). We consider only first order transitions, i.e. transitions involving the crossing of only one saddle point in the PES. This is a reasonable approximation since the probability of higher order transitions is orders of magnitude smaller, at the usual growth temperatures. To calculate the diffusion tensor of In on (1×3), (2×3), and c(4×4) reconstructed wetting layers on GaAs(001) and on the pure InAs(2×4) surface, the PES data are taken from previous studies [17, 13, 14] performed using similar or identical GGA pseudopotentials. From these data the corresponding transition networks have been derived and the In diffusion properties have been calculated.

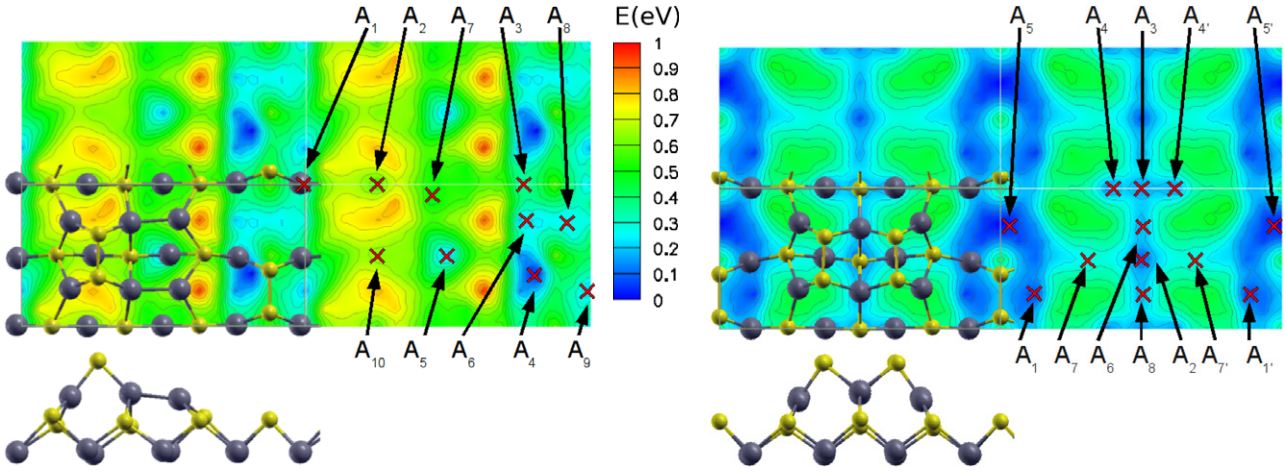

Figure 2. PES for the In adatom on the $\alpha_2(2 \times 4)$ (left) and $\beta_2(2 \times 4)$ (right) surface reconstructions, calculated using the GGA–PBE density functional. The adsorption sites A_i are indicated. Note the effect of the symmetry lowering in α_2 with respect to β_2.

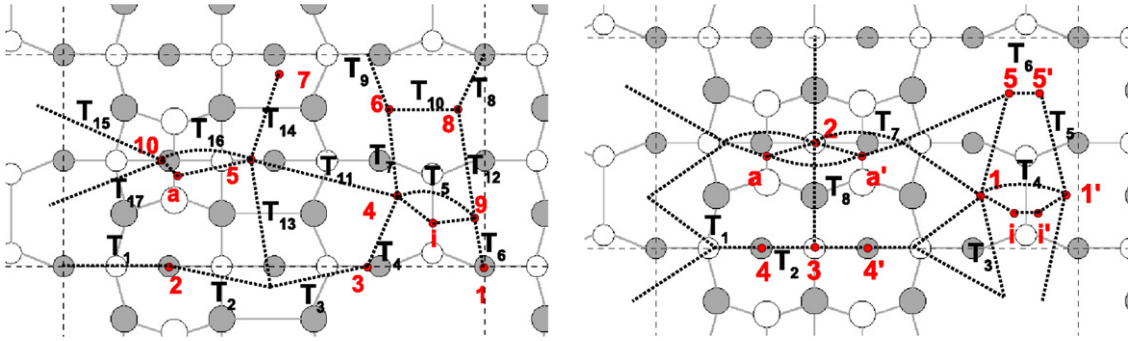

Figure 3. Transition networks within one unit cell for $\alpha_2(2 \times 4)$ (left) and $\beta_2(2 \times 4)$ (right) surface reconstructions. The overall network has the (2×4) periodicity of the surface reconstruction and extends to equivalent minima in neighboring cells. Note the effect of the lower symmetry of α_2 with respect to β_2.

3. Results

3.1. Results for the α_2 and β_2 surface reconstructions of the InAs/GaAs WL: effects of the WL symmetry

The PESs for α_2 and β_2 surface reconstructions are reported in figure 2. The two surfaces are considerably different: the energy difference between the minimum and the maximum values of the PES is about 1 eV for α_2, and much lower, 0.6 eV for β_2. Thus, the β_2 PES is flatter than the α_2 one. Moreover, the PES on β_2 is symmetric with respect a [110] plane while α_2 is not. On both surfaces, low energy trenches are present along the $[\bar{1}10]$ direction, at both sides of the in-dimer chain. These trenches include four adsorption sites each, separated by low confining barriers: this potential landscape should lead to a higher diffusion coefficient along this direction.

We have found ten adsorption sites for In on the α_2 surface reconstruction. The deepest adsorption sites are A_4, A_3, A_8, A_9, and A_5: the first four sites are located in the low energy trench along the $[\bar{1}10]$ direction; the latter adsorption site (A_5) sits on top of the uncovered In atoms at the topmost layer, and it is confined by high barriers.

On the β_2 reconstruction we found instead 12 adsorption sites. The ones with the lowest energies are A_1, $A_{1'}$, A_5, $A_{5'}$, and A_2. The binding site configuration is similar to that found on α_2, but their arrangement follows a more symmetric pattern, due to the higher symmetry of the β_2 reconstruction.

The transition networks derived from the PESs of α_2 and β_2 are shown in figure 3, where the adsorption sites described above are included. For the sites where the adatom is inserted into the ad-dimers we use the label 'a' as indicated in the figure, while for the sites into the in-dimers we use the label 'i'. In the figure, the corresponding transitions to/from neighboring sites are also indicated. Some shallow adsorption sites (e.g. A_6, A_7, $A_{7'}$, A_8) have not been included in the β_2 transition network (figure 3(b)), since the relative confining barriers are lower than 20 meV, and thus, at normal growth temperatures, they are 'invisible' for the random walker. The values for the adsorption sites and confining barriers used in the simulations are reported in tables 1 and 2 for α_2 and β_2 respectively.

We note that α_2 is the WL reconstruction having the lowest symmetry among all the considered reconstructions. Comparison with the β_2 reconstruction which is in many ways similar but has a much higher symmetry can evidence the effects of symmetry. The diffusion coefficients of In on the two surface reconstructions are reported in figure 4. The first observation is that the In diffusion coefficient on β_2 is higher.

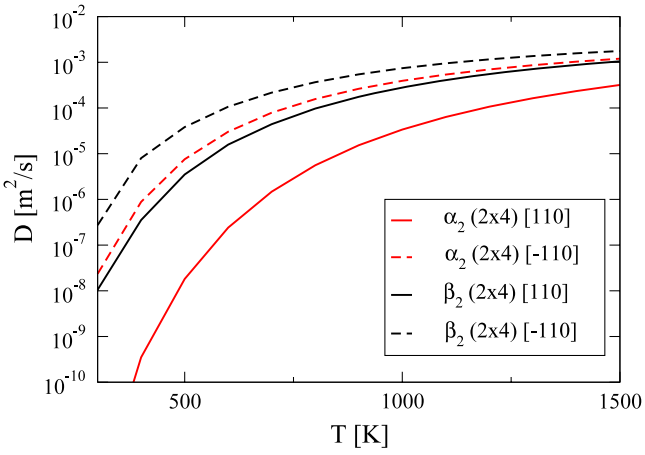

Figure 4. Diffusion coefficients for $\alpha_2(2\times4)$ and $\beta_2(2\times4)$ as a function of the temperature T. Solid lines refer to the [110] direction and dashed lines to the $[\bar{1}10]$ direction.

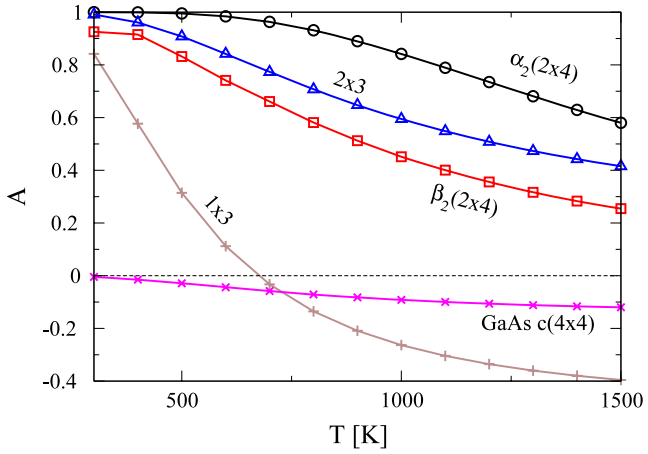

Figure 5. Anisotropy of the diffusion coefficient for the investigated systems, as defined by (5).

Table 1. Energies of adsorption sites (A_n) and barriers (T_n) for In on the $\alpha_2(2\times4)$ surface reconstruction. Energies are expressed in meV. The site A_4 has been chosen as zero of the energy scale.

A_1	A_2	A_3	A_4	A_5	A_6	A_7	A_8	A_9	A_{10}	A_a	A_i
269	546	302	0	115	125	511	193	211	655	737	469
T_1	T_2	T_3	T_4	T_5	T_6	T_7	T_8	T_9	T_{10}	T_{11}	T_{12}
644	754	610	363	477	317	279	335	373	298	628	443
T_{13}	T_{14}	T_{15}	T_{16}	T_{a10}	T_{a5}	T_{i4}	T_{i9}				
602	597	685	684	1337	1209	1254	1144				

Table 2. Energies of adsorption sites (A_n) and barriers (T_n) for In on the $\beta_2(2\times4)$ surface reconstruction. The sites n' for the β_2 are omitted, since they are symmetric to the n sites and have the same energies. Energies are expressed in meV. The site A_5 has been chosen as zero of the energy scale.

A_1	A_2	A_3	A_4	A_5	A_7	A_a	A_i				
104	155	190	212	0	313	386	−40				
T_1	T_2	T_3	T_4	T_5	T_6	T_7	T_8	T_{a2}	T_{aa}	T_{i1}	T_{ii}
437	269	247	288	212	70	362	276	888	979	918	355

This is due to the flatness of the In PES on β_2, as shown in figure 2. We have found that in this case the surface symmetry plays a dominant role in diminishing the PES corrugation, by limiting the atom bond deformation in the surface layer. α_2 is instead more capable to relieve the strain due to the lattice mismatch between the WL and the substrate, by strongly deformating the surface bonds.

We also notice that there is a great difference between the diffusion along the two main surface directions: the In diffusion is much larger along the $[\bar{1}10]$ direction than along the [110] direction, for both surface reconstructions. This is a consequence of the PES shape [18]: low energy regions, with weak energy barriers extending along the $[\bar{1}10]$ direction, act as deep channels for In motion, while along the orthogonal [110] direction the adsorption sites are separated by higher barriers corresponding to the As dimers. This difference can be quantitatively evaluated by defining the anisotropy:

$$A = \frac{D_{[\bar{1}10]} - D_{[110]}}{D_{[\bar{1}10]} + D_{[110]}}. \tag{5}$$

Table 3. Effective diffusion barriers ΔE^* (meV) along the two orthogonal [110] and $[\bar{1}10]$ surface directions.

Surface	$\Delta E^*_{[110]}$	$\Delta E^*_{[\bar{1}10]}$
InAs WL $\alpha_2(2\times4)$	643	337
InAs WL $\beta_2(2\times4)$	375	253
InAs $\beta_2(2\times4)$ [14]	456	386
InGaAs WL (2×3) [17]	259	113
InGaAs WL (1×3) [17]	337	231
GaAs c(4×4) [13]	669	652

The anisotropy for both surfaces is given in figure 5, together with that calculated for the other reconstructions addressed in this work. Of course the anisotropy is higher at low temperatures, since then the probability to overcome high barriers is lower than at high temperatures, thus at low T the diffusion occurs mainly along $[\bar{1}10]$. This means that material transport towards the quantum dots occurs preferentially along the $[\bar{1}10]$ directions.

A further interesting quantity is the effective diffusion barrier ΔE^* along a specified direction. It is obtained from the Arrhenius relation of the diffusion coefficient along specific direction α:

$$D_\alpha = D_\alpha^{(0)} \mathrm{e}^{-\frac{\Delta E^*}{k_B T}}. \tag{6}$$

The effective diffusion barrier gives an indication of the diffusion efficiency along the direction α. In table 3 our results for ΔE^* on α_2 and β_2 are reported together with those obtained for the reconstructions taken from the literature. The $\alpha_2(2\times4)$ reconstruction presents higher effective barriers to In diffusion than the $\beta_2(2\times4)$ reconstruction, in agreement with the obtained lower values of the diffusion coefficient.

The analysis of the site mean occupation time τ_j (4) reported in figure 6 reveals that the sites where the adsorbate spends most of its time are the ones where In is inserted in

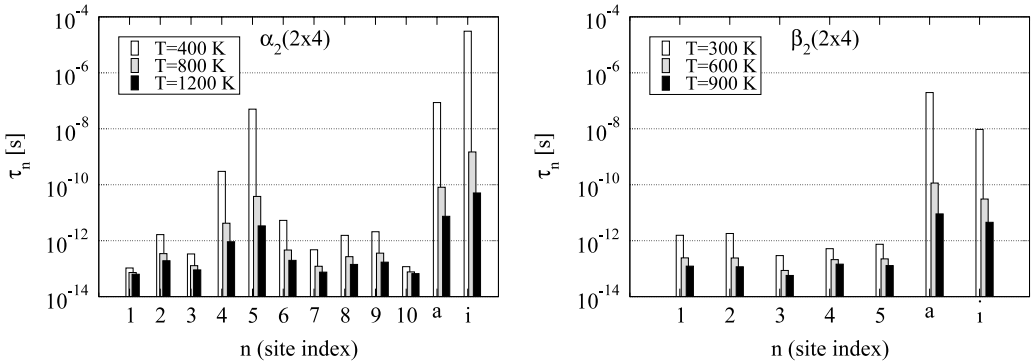

Figure 6. Mean permanence time τ_n for each binding site, for α_2 and for β_2, at different substrate temperatures T. The additional sites where the In adatom is included in the As dimers are labeled by 'a' and 'i' (ad-dimer and in-dimer). The sites n' for the β_2 are not shown in the figure, since they are symmetric to the n sites.

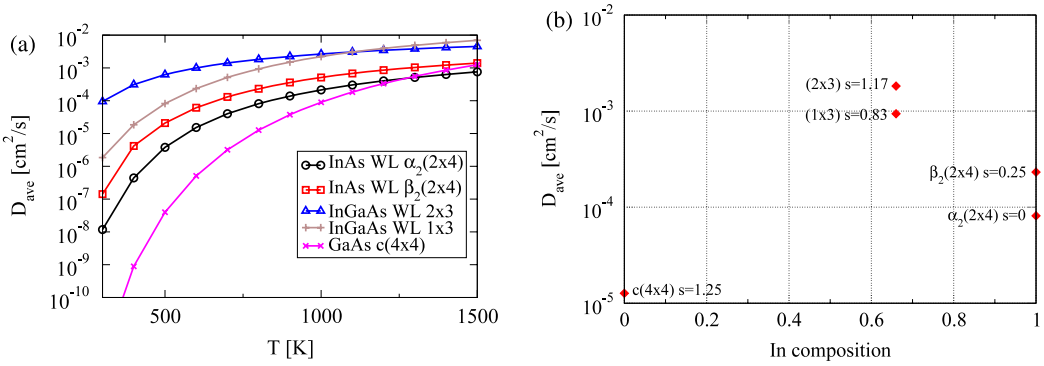

Figure 7. Average diffusion coefficient $D_{\rm ave}$ for the investigated systems: (a) as a function of the temperature, (b) as a function of indium composition and As stoichiometry s, at $T = 800$ K.

the As dimers. Other important high permanence sites are A_1 and A_2 for the α_2 surface reconstruction, and A_4 and A_5 for the β_2 reconstruction [19]. The average permanence time τ_j in the dimer-sites is orders of magnitude higher than that in the other sites, owing to the higher confining barriers. This property allows us to consider these sites as the best candidates for the study of the nucleation process, using the permanence time as an indicator for nucleation. When the temperature is increased, the permanence times tend to become similar for all adsorption sites, because the thermal energy of the adsorbate is higher and the probability to overcome the barriers increases significantly everywhere.

3.2. Effects of the surface composition, reconstruction and strain

In this paragraph we want to discuss the behavior of In diffusion on the In-covered GaAs surfaces by comparing the results for the highly In-covered surface ($\theta \simeq 1.75$ ML) analyzed in the previous paragraph with those obtained for other reconstructions at lower In coverages. We have considered the unstrained clean GaAs(001) c(4 × 4) surface reconstruction [13] and the strained $In_{2/3}Ga_{1/3}As$ WL on GaAs(001) [17] (2 × 3) and (1 × 3) reconstructed. These surface reconstructions have been found [8] to be the most stable at the respective In coverages and phase transitions have been observed taking place during growth between these surface phases at increasing In coverages.

The effect of the adsorption sites sitting in between the As dimers have been discussed in previous works. In the cases of In on c(4 × 4) and on (1 × 3) and (2 × 3), the authors have found these sites too shallow, with a low probability to be occupied at usual growth temperatures, and thus they have not been inserted in the diffusion calculation. On the $\beta_2(2 \times 4)$ surface reconstructions, the in-dimer $A_{\rm i}$ adsorption sites are the ones with the lowest adsorption energy while on the $\alpha_2(2 \times 4)$ the corresponding $A_{\rm i}$ adsorption site has an energy 0.5 eV higher than the PES bottom. Thus, on the β_2 the adsorption sites into the As in-dimer are highly populated, and have to be taken into account for a correct description of In diffusion. On the other hand, on the α_2 surface reconstruction at growth temperatures, the probability to find the adatom in those sites is very low, and their effect on diffusion is therefore negligible. We have verified that the diffusion coefficient is increased only by a factor of 2 on β_2 if the adsorption sites $A_{\rm i}$ and $A_{\rm a}$ are not included in the transition network, while no remarkable difference is found on the α_2.

In figure 7(a) we plot the average In diffusion coefficient $D_{\rm ave} = (D_{[110]} + D_{[\bar{1}10]})/2$ versus T for the different WL reconstructions. In figure 7(b) $D_{\rm ave}$ is shown as a function of the In composition of the WL, which is directly related to the amount of surface strain present on the system. We

notice that the trend of the In diffusion coefficient is not monotonic with the quantity of In incorporated in the WL. The lowest In diffusion coefficient is observed for the c(4 × 4) surface reconstruction, that is the one which is not subjected to compressive strain. For the WL composition available in figure 7(b), In diffusion is highest at 66% In (two orders of magnitude higher than in the previous case), then it decreases again for the (2 × 4) WLs, corresponding to an In coverage of 1.75 monolayers, and 100% In composition. Since the WL reconstructions at 66% In composition are different than those studied at 100% In composition, it is not possible to discriminate the effects on diffusion due to the WL composition, from those due to the particular surface reconstruction.

The anisotropy A, for all the WL reconstructions is reported in figure 5, where we can see that the most anisotropic diffusion tensors are found for In on the $(2 \times N)$ surface reconstructions. This behavior originates from the presence of the in-dimer trenches oriented along the $[\bar{1}10]$ directions having lower barriers for diffusion along $[\bar{1}10]$ (see figure 2).

Finally, we obtain $D_{\text{ave}} = 2.32 \times 10^{-4}$ cm^2 s^{-1} for the β_2 reconstructed WL, and $D_{\text{ave}} = 1.07 \times 10^{-4}$ cm^2 s^{-1} for the clean InAs $\beta_2(2 \times 4)$ surface [14]. Thus the In adatom presents a higher diffusion coefficient on the WL than on the pure InAs surface. In the calculation for the pure InAs [14] the adsorption sites within the in-dimers were not considered (if considered, they would further increase the effective diffusion barriers and make the corresponding diffusion coefficient lower). Indeed, since the InAs WL is compressively strained on GaAs the atom positions are much more displaced from their ideal sites than in the case of the unstrained but reconstructed InAs(001) β_2 surface. Their lateral distance is smaller in the WL than on the free surface, while the interplanar (001) distance is larger. This leads to the flattening of the PES and the In adatom moves more freely on the WL. The trend of the diffusion coefficient which decreases with an increasing compressive strain of the substrate agrees qualitatively with the trends reported in [13].

4. Discussion

This paper provides an overview of In diffusion on InGaAs WLs within the framework of DFT–GGA. The results collected from the literature are complemented by our calculations for the extremely In-rich phases (2 × 4) reconstructed, observed at the onset of the 2D to 3D transition. The trends with the WL reconstruction and composition are outlined.

Our calculations agree with the general behavior experimentally observed. The anisotropy of diffusion is seen to strongly favor the $[\bar{1}10]$ direction. This is consistent with the experimentally observed elongation of self-assembled nanostructures, e.g. in the transformation of InAs quantum dots under slow overgrowth using a GaAs capping layer [28]. Other examples are the formation of mounds elongated along the $[\bar{1}10]$ direction [29] or the formation of elliptical nanorings [30], depending on the deposited GaAs thickness and the annealing time and temperature. The increase of diffusion with In coverage has been observed for In coverage increasing up to the critical thickness [4, 10].

Table 4. Binding energies E_b calculated for the As_2 molecule on the α_2, and for the In atom on α_2 and β_2.

	E_b^{LDA} (eV)	E_b^{GGA} (eV)
As_2	−3.34	−1.80
In on α_2 (A_8)	−2.63	−2.09
In on β_2 (A_5)	−2.75	−2.14

Previous results obtained by us [19] where the In diffusion has been studied within the framework of DFT–LDA, have evidenced some differences with respect to the present ones arising from essentially two factors: (i) DFT–GGA tends to overestimate the lattice mismatch between InAs and GaAs. In our calculations the lattice mismatch is 9.3% for DFT–GGA and 5.3% for DFT–LDA, versus the experimental value of 7.2%. Thus, DFT–GGA overestimates the compressive strain effects, whereas DFT–LDA underestimates them. (ii) DFT–LDA, on the other side, favors binding at highly coordinated sites much more strongly than at low coordination sites [31] (e.g., transition states); thus the adsorbate tends to be more strongly bonded at the minima of the PES and has to overcome higher barriers in a DFT–LDA than in a DFT–GGA description. As an example, we have calculated the binding energy of: (i) the As_2 molecule to α_2, following the reaction $\alpha_2 + As_2 \rightarrow \beta_2$, and (ii) the In adatom in the A_8 (A_5) adsorption site on α_2 (β_2). The results are reported in table 4, where we can see that DFT–LDA produces binding energies per atom 30–40% larger than the corresponding ones calculated by DFT–GGA.

While the topology of the PES is similar with both exchange–correlation functionals, some noticeable differences of the diffusion properties come out of our quantitative calculations. The most important one is the trend of the diffusion coefficient with the number of As dimers on the surface and, as a consequence, the trend of the diffusion coefficient between α_2 and β_2. DFT–LDA predicts an higher diffusion coefficient for the α_2 reconstruction, while DFT–GGA predicts the opposite trend. This is due to the fact that DFT–LDA enhances the effect of In binding into the As dimers and thus, the more As dimers are on the surface, the lower is the diffusion coefficient. DFT–GGA, on the other hand, enhances the effects of the symmetry constraints. β_2, being more symmetric, imposes constraints on the surface lattice relaxation (that is larger for DFT–GGA due to the enhanced lattice mismatch) that leads to a reduction of the surface potential corrugation. Thus, In finds less sites where to be strongly bonded (see figure 2), and this leads to a higher diffusion coefficient for β_2. At the present, the experimental evidences suggest that an high As pressure during MBE growth should suppress In diffusion on the surface [10], agreeing with the LDA provided picture.

Although the obtained energy barriers in LDA and GGA differ significantly, we note that both pictures are compatible with the available experimental data. The mass transport in 3D island formation can be estimated from time-resolved electron diffraction data, as found in [10]. We estimate that an In diffusion coefficient $D > 10^{-10}$ cm^2 s^{-1} is required to account

for the 3D island formation during a growth interruption of 25 s at a sample temperature of 770 K. Both the results calculated in LDA [19] and in GGA exceed the required diffusivity, i.e., both approximations are compatible with experiment. Other attempts to derive the In diffusion constant from an analysis of experimental island densities [32, 33] are model dependent and too inaccurate to discriminate between LDA and GGA activation energy barriers. As a more severe test, one could analyze the As_2 desorption rate in order to compare the apparent activation energy for desorption with our calculated numbers. Again, the available experimental data do not allow us to make a strong statement about the validity of LDA or GGA: while our GGA desorption energy of 1.8 eV is compatible with experiment assuming a conventional pre-exponential factor of 10^{13} s^{-1} [34], our LDA result of 3.34 eV would require an anomalously high pre-exponential factor in the rate law, as reported for InAs(001) in [33]. We believe that realistic values for the As_2 desorption energy should lie somewhere in between our LDA and GGA results. Here, a more reliable experimental determination of the pre-exponential factor would be most helpful to decide about the superiority of the LDA or GGA approximation.

5. Conclusions

We have studied tracer diffusion (of a single In adatom) on $In_xGa_{1-x}As$ WLs deposited on the GaAs(001) substrate. We have considered five different WL reconstructions corresponding to the phases observed sequentially on the surface, during In deposition, starting from the c(4 × 4) reconstruction of the clean GaAs(001) surface, to the $\alpha_2(2\times4)$ and $\beta_2(2\times4)$ reconstructions observed at the In coverage corresponding to the 2D to 3D transition (e.g. nucleation of the quantum dots). The α_2 and the β_2, have also been found to be the most stable for a very high In WL composition [35].

The In diffusion coefficient on $In_xGa_{1-x}As$ WLs has the largest value in the case of the $(N\times3)$ reconstructions, corresponding to $x=\frac{2}{3}$. It is somewhat reduced in the $x=1$ case, corresponding to the β_2 and α_2 reconstructions, but still larger than on the clean GaAs(001) c(4 × 4) surface. This enhanced diffusion on the WL enables the fast self-assembly of quantum dots after the transition to 3D growth. We have also found that the diffusion is highly anisotropic for all the $(2\times N)$ reconstructions, even at very high temperatures, favoring In motion along $[\bar{1}10]$ over [110]. As for the dependence on the compressive strain, we find that, in general, it increases In diffusion.

Moreover, we have found that, in the case of an In-rich WL with β_2 reconstruction, the effect on diffusion of the binding sites within the As dimers is noticeable, while in the case of the α_2 surface reconstruction it can be neglected, as already done in previous studies of In diffusion for the GaAs c(4 × 4), and InGaAs (1×3) and (2×3) reconstructions. Anyway, these adsorption sites acquire a great importance for a further study of nucleation, since they provide a very stable configuration for the In adsorbate.

Finally, we discuss the effect of the employed exchange and correlation potential, V_{xc}, on the quantitative picture of In diffusion, enlightening the different description of the adatom binding properties and the effects of the different GaAs/InAs lattice mismatch provided by the two LDA and GGA methods.

Acknowledgments

We acknowledge the support of the MIUR PRIN-2005 and PRIN-2007, Italy and the European Network of Excellence SANDiE. The calculations were performed at CINECA-Bologna under the grant 'Iniziativa Calcolo Parallelo del CNR-INFM', and at LabCsai in Modena.

References

[1] Stranski I N and Kastranow L 1938 *Sitz.ber., Akad. Wiss. Wien, Math-Nat.wiss. Kl.* IIb **146** 797
[2] Placidi E, Arciprete F, Fanfoni M, Patella F, Orsini E and Balzarotti A 2007 *J. Phys.: Condens. Matter* **19** 225006
[3] Honma T, Tsukamoto S and Arakawa Y 2006 *Japan. J. Appl. Phys.* **45** L777
[4] Patella F, Arciprete F, Placidi E, Nufris S, Fanfoni M, Sgarlata A, Schiumarini D and Balzarotti A 2002 *Appl. Phys. Lett.* **81** 2270
[5] Dayen S A, Yu E T and Wang D 2009 *Nano Lett.* **9** 1967
[6] Grandjean N and Massies J 1993 *J. Cryst. Growth* **134** 51
[7] Bone P A, Ripalda J M, Bell G R and Jones T S 2006 *Surf. Sci.* **600** 973
[8] Belk J G, McConville C F, Sudijono J L, Jones T S and Joyce B A 1997 *Surf. Sci.* **387** 213
[9] Patella F, Arciprete F, Fanfoni M and Balzarotti A 2006 *Appl. Phys. Lett.* **88** 161903
[10] Patella F, Arciprete F, Fanfoni M, Sessi V and Balzarotti A 2005 *Appl. Phys. Lett.* **87** 252101
[11] Ratsch C 2001 *Phys. Rev.* B **63** 161306(R)
[12] Kratzer P, Penev E and Scheffler M 2003 *Appl. Surf. Sci.* **216** 436
[13] Penev E, Kratzer P and Scheffler M 2001 *Phys. Rev.* B **64** 085401
[14] Fujiwara K, Ishii A and Aisaka T 2004 *Thin Solid Films* **464–465** 35
[15] Kley A, Ruggerone P and Scheffler M 1997 *Phys. Rev. Lett.* **79** 5278
[16] LePage J G, Alouani M, Dorsey D L, Wilkins J W and Blöchl P E 1998 *Phys. Rev.* B **58** 1499
[17] Penev E, Stojkovic S, Kratzer P and Scheffler M 2004 *Phys. Rev.* B **69** 115335
[18] Rosini M, Magri R and Kratzer P 2008 *Phys. Rev.* B **77** 165323
[19] Rosini M, Righi M C, Kratzer P and Magri R 2009 *Phys. Rev.* B **79** 075302
[20] Perdew J P, Burke K and Ernzerhof M 1996 *Phys. Rev. Lett.* **77** 3865
[21] Mills G, Jónsson H and Schenter G 1994 *Phys. Rev. Lett.* **72** 1124
[22] Haus J W and Kehr K W 1987 *Phys. Rep.* **150** 263
[23] Festa R and Galleani E 1978 *Physica* A **90** 229
[24] Smoluchowski M v 1915 *Ann. Phys. Lpz.* **48** 1103
[25] Schnakenberg J 1976 *Rev. Mod. Phys.* **48** 571
[26] Pechukas P 1976 *Dynamics of Molecular Collisions, Part B* ed W H Miller (New York: Plenum)
[27] Truhlar D G, Hase W L and Hynes J T 1983 *J. Phys. Chem.* **87** 2664
[28] Costantini G, Rastelli A, Manzano C, Acosta-Diaz P, Songmuang R, Katsaros G, Schmidt O G and Kern K 2006 *Phys. Rev. Lett.* **96** 226106

[29] Patella F, Nufris S, Arciprete F, Fanfoni M, Placidi E, Sgarlata A and Balzarotti A 2003 *Phys. Rev.* B **67** 205308
[30] Sztucki M, Metzger T H, Chamard V, Hesse A and Holy V 2006 *J. Appl. Phys.* **99** 033519
[31] Kratzer P, Morgan C G and Scheffler M 1998 *Prog. Surf. Sci.* **59** 135
[32] Shiramine K, Itoh T, Muto S, Kozaki T and Sato S 2002 *J. Cryst. Growth* **242** 332
[33] Madhukar A, Ramachandran T R, Konkar A, Mukhametzhanov I, Yu W and Chen P 1998 *Appl. Surf. Sci.* **123/124** 266
[34] Banse B A and Creighton J R 1992 *Appl. Phys. Lett.* **60** 856
[35] Penev E 2002 On the theory of surface diffusion in InAs/GaAs(001) heteroepitaxy *PhD Thesis* Technische Universität Berlin